

N-Heterocyclic Carbene-Catalyzed Chemo- and Enantioselective Three-Component Esterification/Amidation Relay for Access to Planar Chiral Ferrocene Derivatives

Youlin Deng,^{||} Xinghua Wang,^{||} Haitao Liu, Hui Cai, Chaoyang Song, Yonggui Robin Chi, Donghui Wei,* and Zhichao Jin*



Cite This: *ACS Catal.* 2025, 15, 6130–6140



Read Online

ACCESS |



Metrics & More



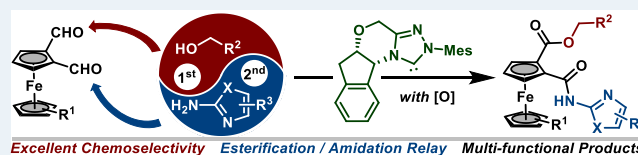
Article Recommendations



Supporting Information

ABSTRACT: An *N*-heterocyclic carbene (NHC)-catalyzed three-component esterification/amidation relay strategy was disclosed for facile access to enantio-enriched planar chiral ferrocene derivatives. The esterification and amidation reactions in the catalytic relay proceeded in sequence in both chemoselective and enantioselective fashions. Both experimental and computational methods were used to reveal the reaction mechanism and indicated that both the hydrogen-bonding (H-bonding) interactions and the basic additives in the catalytic system had played crucial roles in the reaction chemo- and stereoselectivities. The planar chiral ferrocene-based ester–amide products showed interesting applications in the synthesis of multiple novel ligands for asymmetric catalysis and the development of chiral bactericides for crop protection.

KEYWORDS: ferrocenes derivatives, planar chirality, *N*-heterocyclic carbene, asymmetric synthesis



INTRODUCTION

Ferrocene derivatives have found significant applications in medicinal chemistry (Figure 1a, top side).^{1–8} Typical examples could be found in the applications of the ferrocenone,⁹ ferrocifen,¹⁰ and ferroquine.¹¹ The ferrocenone was used in the former USSR in the 1970s for the treatment of anemia. The ferrocifen is a hybrid of ferrocene and tamoxifen, which represents one of the most efficient molecules against both hormone-dependent and hormone-independent breast cancer cell lines. The planar chiral ferroquine has shown good activities against both chloroquine-sensitive and chloroquine-resistant strains of *Plasmodium falciparum*, which has been identified as the most promising lead structure for antimalaria drug development. In addition, the optically active multifunctional ferrocenes bearing stereogenic planes have been extensively used as excellent ligands and catalysts in asymmetric synthesis (Figure 1a, bottom side).^{12–25} For example, Fu developed a series of chiral DMAP-derivatives based on the ferrocene scaffold as nucleophilic catalysts or ligands for asymmetric synthesis.²² The Josiphos contains two trivalent phosphine groups on the planar chiral ferrocene structure, which represents one of the most efficient and versatile bidentate phosphine ligands in asymmetric hydrogenation, hydroacylation, and other reactions.^{26,27} Scheidt and co-workers proved that the planar chiral ferrocene could be transformed into imidazolium-derived *N*-heterocyclic carbenes, which could be used as both effective organocatalysts for asymmetric cycloaddition reactions and excellent chiral ligands for nickel and copper catalysis.²⁸ Therefore, the development

of facile approaches for direct access to enantio-enriched planar chiral functional ferrocenes is of great significance and urgency.

A diversity of catalytic approaches have been developed in the past decade for facile access to planar chiral ferrocene molecules (Figure 1b).²⁹ Dramatic success has been achieved in the transition-metal-catalyzed asymmetric C–H activation on the cyclopentadienyl ring of the ferrocene scaffold.^{30–42} With the assistance of the directing group (DG) installed on the ferrocene backbone, additional functional groups including alkyl,³⁸ aryl,³⁵ alkynyl,^{36,42} alkenyl,⁴⁰ acyl,³⁹ acyloxy,³⁹ amido,³² and boryl³⁴ groups could be efficiently introduced to the *o*- or *m*-position to the DG in enantioselective fashion under the catalysis of transition-metal/chiral ligand systems. Meanwhile, the side chains on the ferrocene structure could go through asymmetric addition reactions to give the planar chiral products through kinetic resolutions, desymmetrizations, or enantioselective cascade ring-closing processes.^{43–45} To the best of our knowledge, the asymmetric catalytic synthesis of planar chiral molecules has been focused on two-component reactions. Three-component catalytic reactions with different transformations occurring in sequence have not been

Received: December 7, 2024

Revised: March 24, 2025

Accepted: March 25, 2025

Published: April 1, 2025



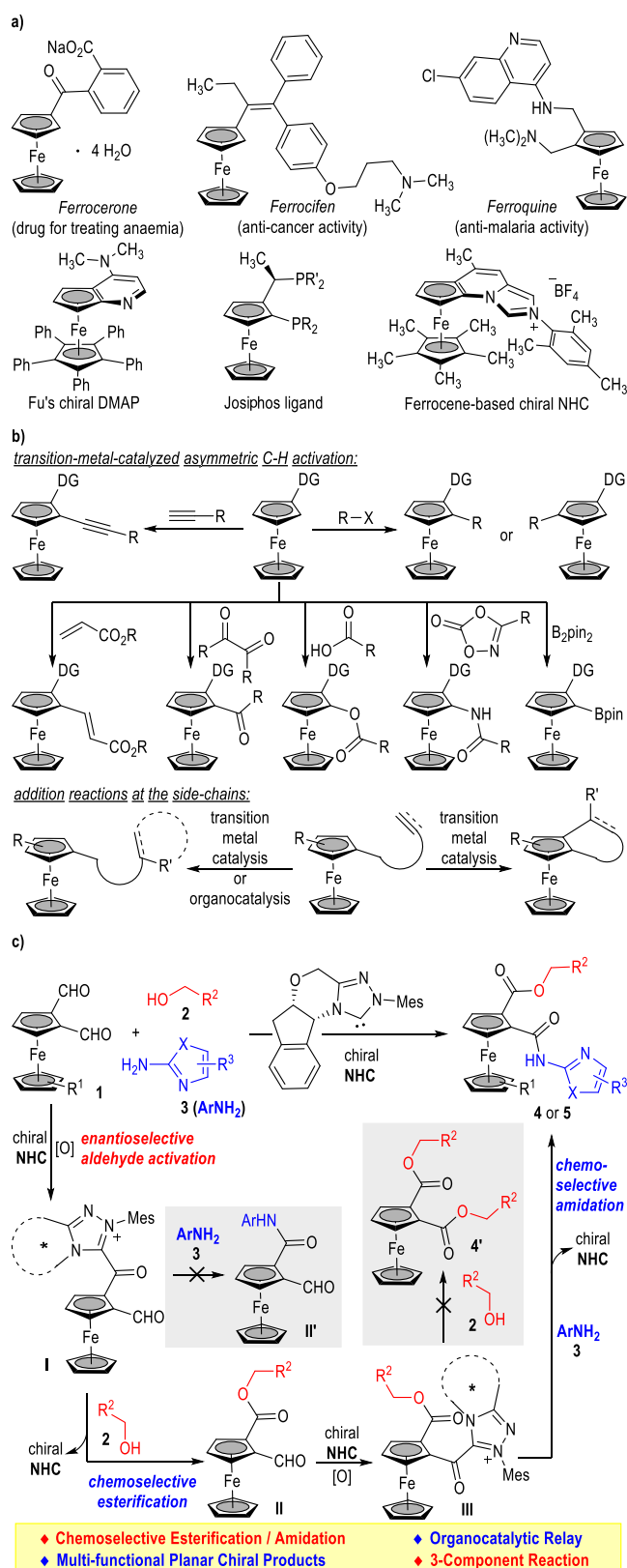


Figure 1. Application of ferrocene derivatives and catalytic methods for access to planar chiral ferrocenes. (a) Ferrocene derivatives in medicinal and synthetic chemistry. (b) Catalytic approaches for access to planar chiral ferrocenes. (c) This work: multicomponent organocatalytic relay for access to chiral ferrocenes.

developed for planar chirality introduction. In addition, although significant progress in the preparation of planar chiral ferrocene derivatives has been achieved with transition-metal catalysis, success in the organocatalyzed asymmetric synthesis of planar chiral ferrocenes is rather limited.^{29,46}

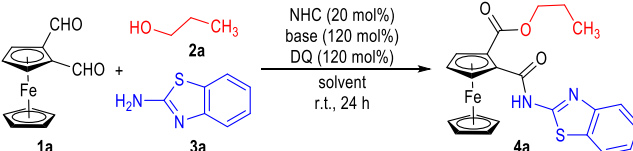
As a continuous effort in our group on the development of organocatalytic multicomponent parallel or relay reactions for planar chiral molecular synthesis,^{46–48} we herein disclose an *N*-heterocyclic carbene (NHC)-catalyzed three-component esterification/amidation relay method for the facile access to enantio-enriched planar chiral ferrocene derivatives (Figure 1c). Typically, the pro-chiral ferrocene-dicarbaldehyde **1** could be enantioselectively activated by the chiral NHC catalyst to give the acylazolium intermediate **I**, which could chemo-selectively react with the alcohol substrate **2** to give the monoester intermediate **II**.⁴⁹ The chiral monoester intermediate **II** could be further activated by the same NHC catalyst to form the acylazolium intermediate **III**, which could then be captured by the heteroaryl amine **3** to afford the final product **4** (or **5**) in chemo- and enantioselective fashion.

It is worth noting that the chemo- and enantioselective esterification and amidation reactions occurred in a sequential manner. The amide monoaldehyde intermediate **II'** and the diester byproduct **4'** were not observed in this reaction. H-bonding interactions between the ester group of the intermediate **III** and the amine substrate **3** were believed vital to the chemoselectivities of the current catalytic relay.

RESULTS AND DISCUSSION

Reaction Development. We commenced the condition optimization of the NHC-catalyzed desymmetrization reaction^{50–66} using the ferrocene dicarbaldehyde **1a**, propanol **2a**, and 2-aminobenzothiazine **3a** as the reaction starting materials (Table 1). Chiral aminoindanol-derived NHC catalysts were tested in the presence of stoichiometric amounts of the base Cs₂CO₃ and the DQ oxidant in the solvent of dichloromethane (entries 1–5). The NHC catalysts bearing electron-rich *N*-aryl groups were found to be efficient for this transformation, with the target planar chiral ester–amide bifunctional product **4a** afforded in good yields and enantioselectivities (entries 1–2). Switching the electron-rich *N*-aryl group on the NHC catalyst into electron-deficient ones resulted in significant drops on the product yield (entries 3–4). To our delight, replacing the BF₄[−] anion of the pre-NHC catalysts with Cl[−] resulted in additional improvement on both the product yield and optical purity (entry 5). All the other organic and inorganic bases we tested failed to promote either the yield or enantioselectivity of the NHC-catalytic relay (e.g., entries 6–8). The catalytic enantioselective esterification/amidation relay could be carried out in a variety of organic solvents, although the products were generally afforded with relatively lower yields or optical purities (entries 9–11). It is worth noting that only 1.2 equiv. of the DQ oxidant was needed for the two-step oxidative esterification/amidation catalytic relay. Both the oxygen in the air and the ferrocene unit were believed to be responsible for the effective oxidation process in the second step of amidation reaction (for control experiments and postulated mechanism, see Supporting Information).^{31,67–70}

Reaction Scope. With an optimal catalytic condition at hand, we then examined the reaction scope using the ferrocene dicarbaldehyde **1**, alcohol **2**, and the heteroaryl amine **3** bearing different substituents and substitution patterns (Figure 2).

Table 1. Optimization of Reaction Conditions^a


A: Ar = Mes;
 B: Ar = Ph;
 C: Ar = C₆F₅
 D: Ar = C₆H₂Cl₃

entry	NHC	base	solvent	yield (%) ^b	er ^c
1	A	Cs ₂ CO ₃	CH ₂ Cl ₂	85	93:7
2	B	Cs ₂ CO ₃	CH ₂ Cl ₂	86	85:15
3	C	Cs ₂ CO ₃	CH ₂ Cl ₂	41	55:45
4	D	Cs ₂ CO ₃	CH ₂ Cl ₂	63	84:16
5	E	Cs ₂ CO ₃	CH ₂ Cl ₂	87	96:4
6	E	K ₃ PO ₄	CH ₂ Cl ₂	79	94:6
7	E	DIEA	CH ₂ Cl ₂	60	75:25
8	E	DBU	CH ₂ Cl ₂	0	0
9	E	Cs ₂ CO ₃	THF	<5	
10	E	Cs ₂ CO ₃	toluene	71	82:18
11	E	Cs ₂ CO ₃	CH ₃ CN	80	89:11

^aReaction conditions: **1a** (0.2 mmol), **2a** (0.4 mmol), **3a** (0.3 mmol), catalyst (0.04 mmol), DQ (0.24 mmol), base (0.24 mmol), and solvent (2.0 mL) at r.t for 24 h. ^bIsolated yield of **4a**. ^cThe er values were determined via HPLC on the chiral stationary phase.

Both electron-donating and electron-withdrawing groups could be installed on the 6-position of the 2-aminobenzothiazole substrate **3a** without much erosion on the reaction yields or enantioselectivities (e.g., **4b** to **4i**). Similarly, introducing substituents on the 5-position of the 2-aminobenzothiazole substrate **3a** led to little influence on the reaction outcome (e.g., **4j** to **4q**). In addition, substitution on the 4-position of the 2-aminobenzothiazole substrate **3a** resulted in similar product yields and optical purities (e.g., **4r** to **4t**). The 2-aminobenzothiazole substrate bearing a 7-carboxylate group could also give the target product **4u** in an excellent yield and good enantioselectivity. Interestingly, the benzothiazole ring of substrate **3a** could be switched into a substituted thiazole group or a substituted oxazole group, with the desired products afforded in good yields with good to excellent optical purities (**4v** to **4w**). Switching the 2-aminothiazole substrates in the current oxidative esterification/amidation relay into aniline, benzylamine, butylamine, dimethylamine, or 2-aminopyridine resulted in no formation of the target planar chiral ester–amide bifunctional ferrocene products. The acidities of the amino groups in the substrates were believed to be responsible for their reactivities in the second step of the amidation reaction: the 2-aminothiazole substrates are more acidic than the other amines and could provide stronger H-bonding interactions with both the base Cs₂CO₃ and the key transition states throughout the reaction process to substantially decrease the energy barriers in the catalytic oxidative amidation reaction (for details, see Supporting Information).⁷¹

Linear alcohols with different lengths ranging from 2 to 11 carbons could give the planar chiral ester–amide products in generally good yields with good to excellent enantioselectivities (**5a** to **5j**). Branched alcohols such as isobutanol could give the

target product **5k** in a good yield and enantioselectivity. Cyclic alcohol such as cyclobutanol gave the product **5l** in a relatively lower yield and optical purity. It should be noted that the regular secondary and tertiary alcohols we tested (e.g., isopropanol, tert-butanol, 1,1-diphenyl methanol) in this catalytic relay were not effective under the current reaction condition. The substantially increased steric hindrance in the secondary and tertiary alcohols might prevent their nucleophilic additions to the acylazolium intermediates in the oxidative esterification step. Replacing the alcohol substrates **2** with phenols or thiols led to the formation of the diesters or dithioesters as the main products, with the target ester–amide or thioester–amide products afforded in 0–6% yields under the current catalytic condition (for details, see Supporting Information).

Alkyl groups with various substitution patterns were also well tolerated on the cyclopentadienyl ring of the ferrocene dicarbaldehyde substrate. For instance, both linear and branched alkyl groups with different lengths gave the desired planar chiral products in generally satisfactory yields and enantioselectivities (e.g., **5m** to **5p**). A phenyl group could also be installed on the terminal side of the alkyl chain on the ferrocene group without obvious erosion on the reaction yield, although the optical purity of the product was a bit decreased (**5q** to **5r**).

Mechanistic Study. We carried out several control experiments to shed light on the reaction mechanism (Figure 3). First of all, we respectively examined the feasibilities of the monoesterification and the monoamidation reactions of the ferrocene dicarbaldehyde substrate **1a** (Figure 3a). Under the currently optimized reaction condition, the monoesterification of **1a** occurred smoothly to give the planar chiral ferrocene monoester intermediate (*R*)-**6** in an excellent yield and enantioselectivity (eq 1). However, the monoamidation of **1a** with the 2-aminobenzothiazole substrate **3a** could not happen under the same reaction condition (eq 2). Therefore, the asymmetric catalytic relay was believed to be initiated by the NHC-catalyzed oxidative esterification reaction with the alcohol substrates.

Second, we checked the reactivity of the chiral monoester intermediate (*R*)-**6** in the esterification and the amidation reactions (Figure 3b). It is interesting to find that the second esterification of the monoester intermediate (*R*)-**6** could not happen under the same reaction conditions as the previous step (eq 3). In stark contrast, the amidation reaction of monoester (*R*)-**6** occurred smoothly to give the final product in an excellent yield and enantioselectivity (eq 4). Therefore, the catalytic relay was proved to be a chemoselective cascade esterification and amidation process.

After that, we examined the enantiocontrol in the second amidation reaction through the kinetic resolution (KR) of the racemic ferrocene monoester intermediate (rac)-**6** (Figure 3c). Under the current catalytic condition, (rac)-**6** could react with 0.5 equiv of the 2-aminobenzothiazole substrate **3a** to give the target product **4a** in a 48% yield with poor enantioselectivity. The remaining ferrocene substrate **3a** was also obtained in a poor er value from the KR process. Therefore, the enantio-determining step was believed to lie in the first esterification step.

The linear relationship between the ee values of the NHC catalyst and the product revealed that only one molecule of the NHC catalyst was involved in the enantio-determining step for the esterification/amidation relay (Figure 3d).

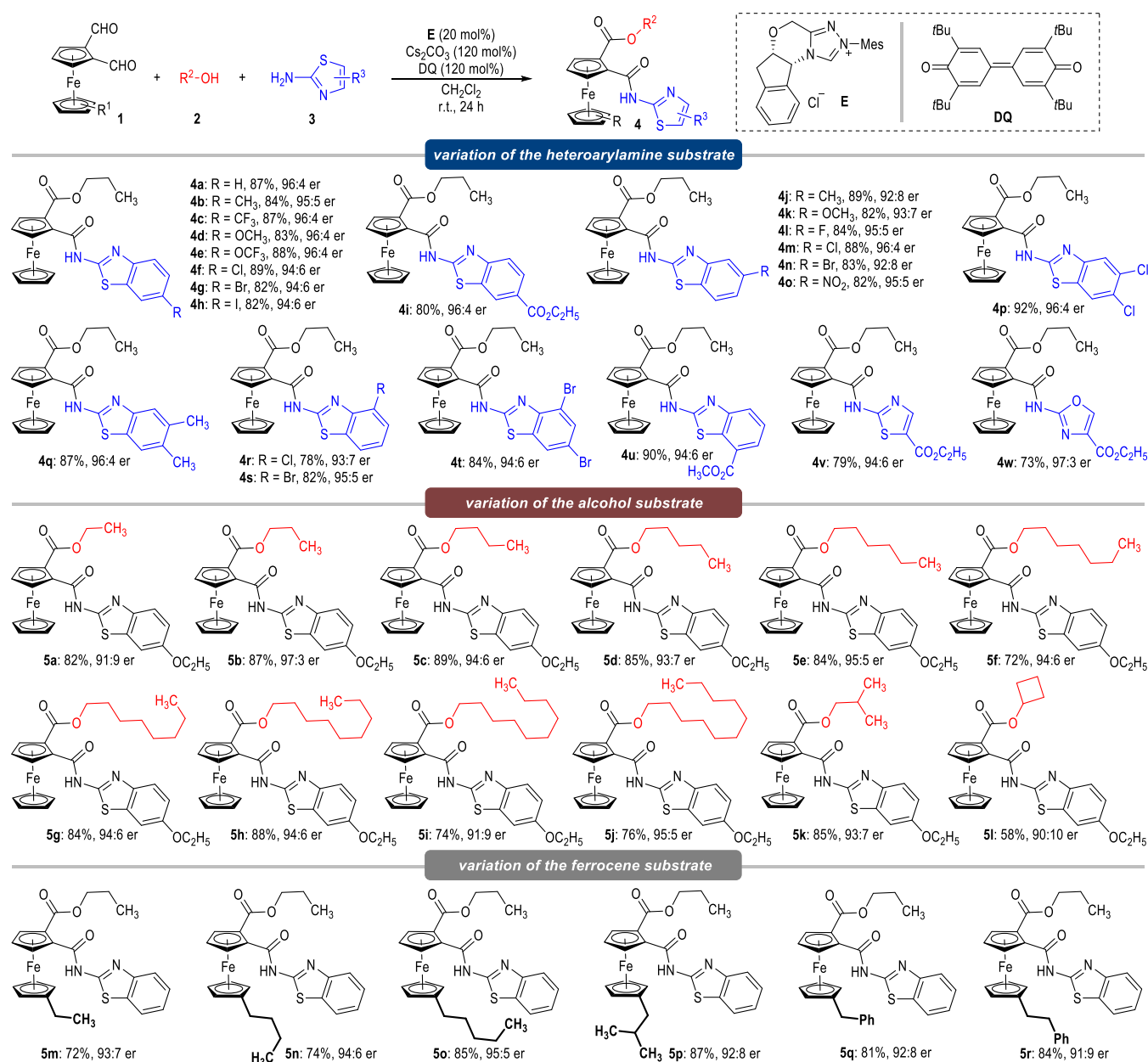


Figure 2. Substrate scope of the NHC-catalyzed enantioselective esterification/amidation relay.

DFT calculations at the B3LYP-D3BJ/6-311 + G(d,p)(SDD for Fe and Cs)/SMD_{dichloromethane}//B3LYP-D3BJ/def2-SVP/SMD_{dichloromethane} level provided further insights into the reaction mechanism (Figures 4 and 5). Detailed computational results and discussion on stereoselectivity are given in the Supporting Information. The reaction can be divided into two stages, i.e., oxidative esterification and oxidative amidation. As shown in Figure 4, the first stage is initiated with the nucleophilic addition of NHC to **1a** via transition state **TS1** ($\Delta G^\ddagger = 18.0$ kcal/mol), forming zwitterionic intermediate **M1**. With the assistance of CsHCO_3 , a [1,2]-proton transfer of **M1** occurs to form intermediate **M2** via transition state **TS2** ($\Delta G^\ddagger = 5.3$ kcal/mol). **M2** is then oxidized by oxidant **DQ** to produce cationic intermediate **M3** via transition state **TS3** ($\Delta G^\ddagger = 6.3$ kcal/mol). Subsequently, **M3** combines with **3a**- CsCO_3^- to form the precursor **preTS4'** with an exotherm of 8.0 kcal/mol. The precursor **preTS4'** can exchange substrates **2a** and **3a** to form the precursor **preTS4** with an endotherm of

8.4 kcal/mol. Both precursors **preTS4** and **preTS4'** can pass through transition states **TS4** ($\Delta G^\ddagger = 0.9$ kcal/mol) and **TS4'** ($\Delta G^\ddagger = 15.4$ kcal/mol) to generate intermediates **M4** and **M4'**, respectively. Following this, intermediates **M4** and **M4'** undergo catalyst regeneration to produce intermediates **M5** and **M5'** via **TS5** ($\Delta G^\ddagger = 3.5$ kcal/mol) and **TS5'** ($\Delta G^\ddagger = 14.7$ kcal/mol), separately. Since the transition states **TS4** and **TS5** are both lower in energy compared to **TS4'** and **TS5'**, substrate **1a** preferentially undergoes oxidative esterification, leading to the formation of intermediate **M5**.

Similar to the first stage, in the second stage, intermediate **M5** undergoes nucleophilic addition of NHC, [1,2]-proton transfer, and oxidation of **DQ** to obtain intermediate **M8** via transition states **TS6** ($\Delta G^\ddagger = 19.2$ kcal/mol), **TS7** ($\Delta G^\ddagger = 5.8$ kcal/mol), and **TS8** ($\Delta G^\ddagger = 4.8$ kcal/mol), respectively (Figure 5). Intermediate **M8** then combines with **3a**- CsCO_3^- to give precursor **preTS9'**, which can be transformed into precursor **preTS9'** through the exchange of **2a** and **3a**,

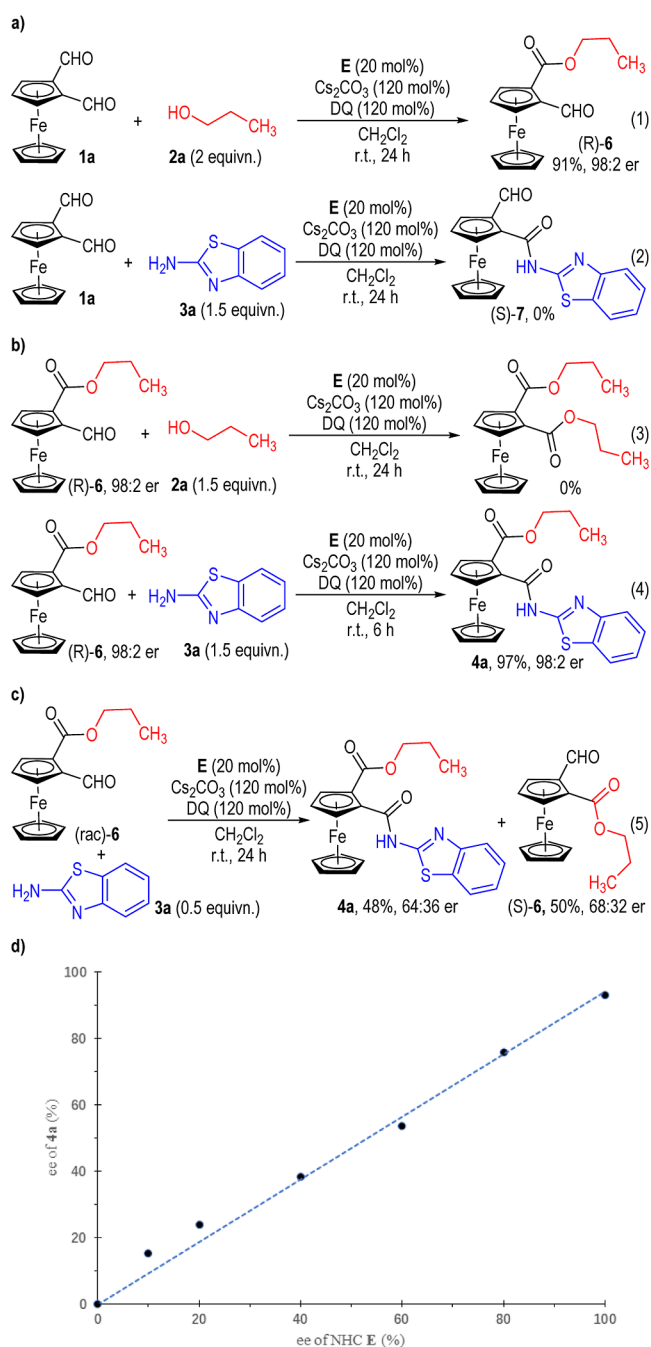


Figure 3. Control experiments for the NHC-catalyzed oxidative esterification/amidation relay. (a) Esterification and amidation reactions of the ferrocene dicarbaldehyde **1a**. (b) Esterification and amidation reactions of the chiral mono-ester intermediate **(R)-6**. (c) Kinetic resolution of the racemic mono-ester intermediate **6**. (d) Relationship between the product ee and the catalyst ee values.

requiring an endotherm of 12.0 kcal/mol. Precursors preTS9 and $\text{preTS9}'$ subsequently convert to intermediates **M9** and **M9'** via transition states **TS9** ($\Delta G^\ddagger = 12.2$ kcal/mol) and **TS9'** ($\Delta G^\ddagger = 3.7$ kcal/mol), respectively. Finally, intermediates **M9** and **M9'** undergo catalyst regeneration, generating the product **4a** and byproduct **4a'** via transition states **TS10** ($\Delta G^\ddagger = 0.6$ kcal/mol) and **TS10'** ($\Delta G^\ddagger = 0.5$ kcal/mol), respectively. Because transition states **TS9** and **TS10** are lower in energy compared to **TS9'** and **TS10'**, intermediate **M5** preferentially

undergoes oxidative amidation, resulting in the formation of product **4a**.

Control experiments indicate that neither the first-stage amination nor the second-stage esterification process can proceed (Figure 3, eqs 2 and 3), suggesting that the overall activation free energy associated with transition states **TS4'** and **TS9'** exceeds 25 kcal/mol. These transition states involve not only nucleophilic addition but also proton transfer, highlighting the limitations of explaining their reactivity solely based on the nucleophilicity of amine and alcohol substrates.^{72,73} Furthermore, given that CsCO_3^- can also function as a nucleophile, potentially competing with amine and alcohol substrates, it is necessary to consider the possibility of its reaction with acylazolium intermediates **M3** and **M8** in two stages. As illustrated in Figure 6, the calculated results indicate that in the first stage, CsCO_3^- can function as a nucleophile, reacting with the acylazolium intermediate **M3** through transition states **TS4''** and **TS5''** to form intermediate **M5''**, which subsequently converts into intermediate **M6''** (Figure 6, left side). Comparing with intermediate **M6''**, the activation free energies of transition states **TS4** and **TS4'** are 22.3 and 28.4 kcal/mol, respectively (Figure 4). This suggests that when compound **1a** is used as the substrate and the amine **3a** as the nucleophile, the reaction cannot proceed via transition state **TS4'** at room temperature. Similarly, in the second stage, the reaction preferentially proceeds through carbonate acting as the initial nucleophile, reacting with the acylazolium intermediate **M8** to generate intermediates **M10''** and **M11''** (Figure 6, right side). Compared to the free energy of intermediate **M11''**, the relative free energies of transition states **TS9** and **TS9'** increase to 22.1 and 25.6 kcal/mol, respectively (Figure 5). This provides an explanation for why the reaction between **M5** and alcohol **2a** does not occur.

In addition, we have also analyzed and compared the geometric configurations of the transition states **TS4'**, **TSS'**, **TS9**, and **TS10** in the oxidative amidation processes of the two different stages (Figure 7). Compared with the oxidative amidation transition states **TS4'** and **TSS'** in the first stage (Figure 7a), there is one more N–H...O hydrogen bonding interaction in the oxidative amidation transition states **TS9** and **TS10** in the second stage (Figure 7b), which greatly stabilizes transition states **TS9** and **TS10**. Therefore, the Gibbs free energies of the transition states involved in the second amidation process are relatively lower.

Synthetic Applications of the Afforded Planar Chiral Ester–Amide Product. The planar chiral ester–amide product **4a** obtained from this NHC-catalyzed oxidative esterification/amidation relay contains multiple functionalities and can be transformed into interesting structures with promising utilities in asymmetric synthesis (Figure 8). For example, the free amide N–H group of **4a** could be blocked by a methyl group to give **8** in a good yield and optical purity (Figure 8a). The ester group on **4a** could easily be hydrolyzed under basic conditions to give the planar chiral acid **9** in an almost quantitative yield. Simple amidation reaction of **9** led to the formation of the planar chiral diamide products **10**, **11**, and **12** in good to excellent yields and enantioselectivities. It is worth noting that the planar chiral product **12** contains a bioactive fragment of the anesthetic drug of benzocaine.

The above optically enriched planar chiral compounds possess interesting chiral scaffolds with multiple H-bonding donor units. Therefore, we examined the reactivities of these compounds as chiral ligands in several trans-metal-catalyzed

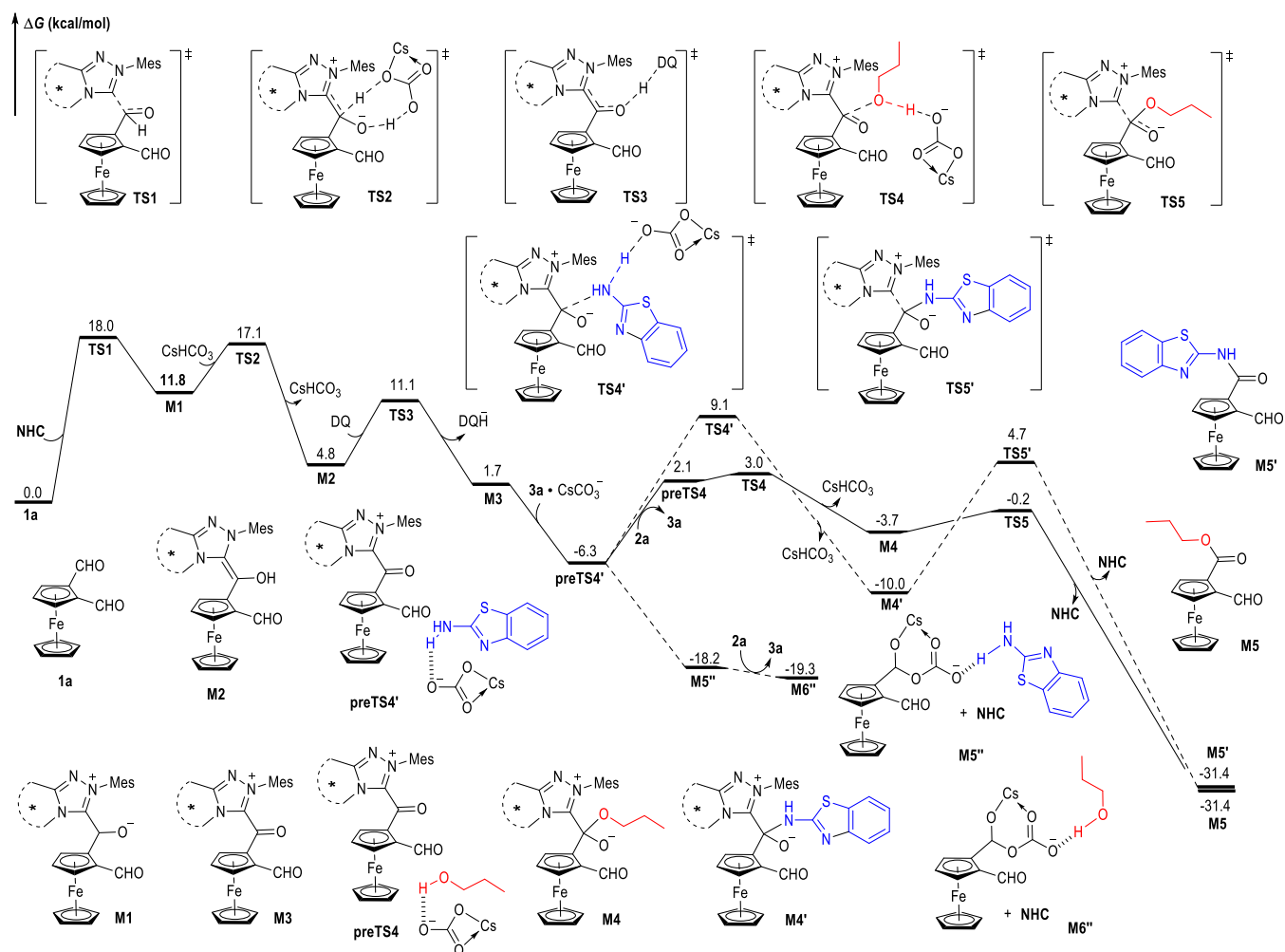


Figure 4. Gibbs free energy profiles for the NHC-catalyzed esterification/amidation relay in the first stage.

asymmetric reactions (Figure 8b). The planar chiral ferrocene-based carboxylic acid **9** could facilitate the palladium-catalyzed asymmetric allelic alkylation reaction between the malonate **13** and the alkene **14**, with the chiral product **15** afforded in a moderate yield and optical purity (Figure 8b, eq 1).^{74,75} The enantioselective reduction of the imine **16** is the key step in the asymmetric synthesis of the classical herbicide (*S*)-metolachlor (Figure 8b, eq 2).^{76–78} With planar chiral diamide compound **11** used as the ligand, secondary amine product **17** could be afforded in a moderate yield and er value.

Antibacterial Activities of the Planar Chiral Ferrocene Derivatives against Plant Pathogens. Thiazole is a common core structure in various antibacterial pesticide molecules.^{79,80} We were very interested in the potent applications of planar chiral ferrocene-based thiazole derivatives **4** and **5** afforded from the current NHC-catalyzed three-component relay reactions. *Xanthomonas oryzae* pv *oryzae* (*Xoo*)^{81–83} is a devastating bacterium affecting rice and has led to severe damage to rice harvests worldwide. Controlling the leaf blight disease caused by *Xoo* in plants has been challenging, as there are few drugs available in the market for this purpose. Consequently, we tested the *in vitro* antibacterial activities of the planar chiral ferrocene derivatives against *Xoo* (Table 2).

Several of the *R_p*-enantiomers of the planar chiral ferrocene derivatives (e.g., *R_p*-**4p**, *R_p*-**4v**, and *R_p*-**5c**) showed better

antibacterial activities than the commercial bactericides of Bismethiazol (BT) and Thiodiazole Copper (TC). It is also interesting to find that the *R_p*-enantiomers exhibited better activities than their enantiomers and the racemates. The planar chiralities of the ferrocene structures appeared to play critical roles in their bactericidal activities, which might provide novel interactions between the pesticide molecules and the target proteins in either the plant cells or the pathogens.

CONCLUSIONS

In summary, we have developed an NHC-catalyzed chemo- and enantioselective three-component esterification/amidation relay for efficient synthesis of planar chiral ferrocene derivatives. A wide range of functionalities were well tolerated on all the starting materials, with the ferrocene-based bifunctional ester/amide products afforded in generally good to excellent yields and enantioselectivities under mild conditions. It is worth noting that the esterification and amidation reactions proceeded in sequence in the current protocol. Experimental and computational studies revealed that the H-bonding interaction between the ferrocene-based monoaldehyde intermediate and the amine substrate was critical for the chemoselectivity. The planar chiral ferrocene derivatives obtained from this approach also showed interesting synthetic and bioactive applications. Ongoing studies include the development of novel catalytic strategies

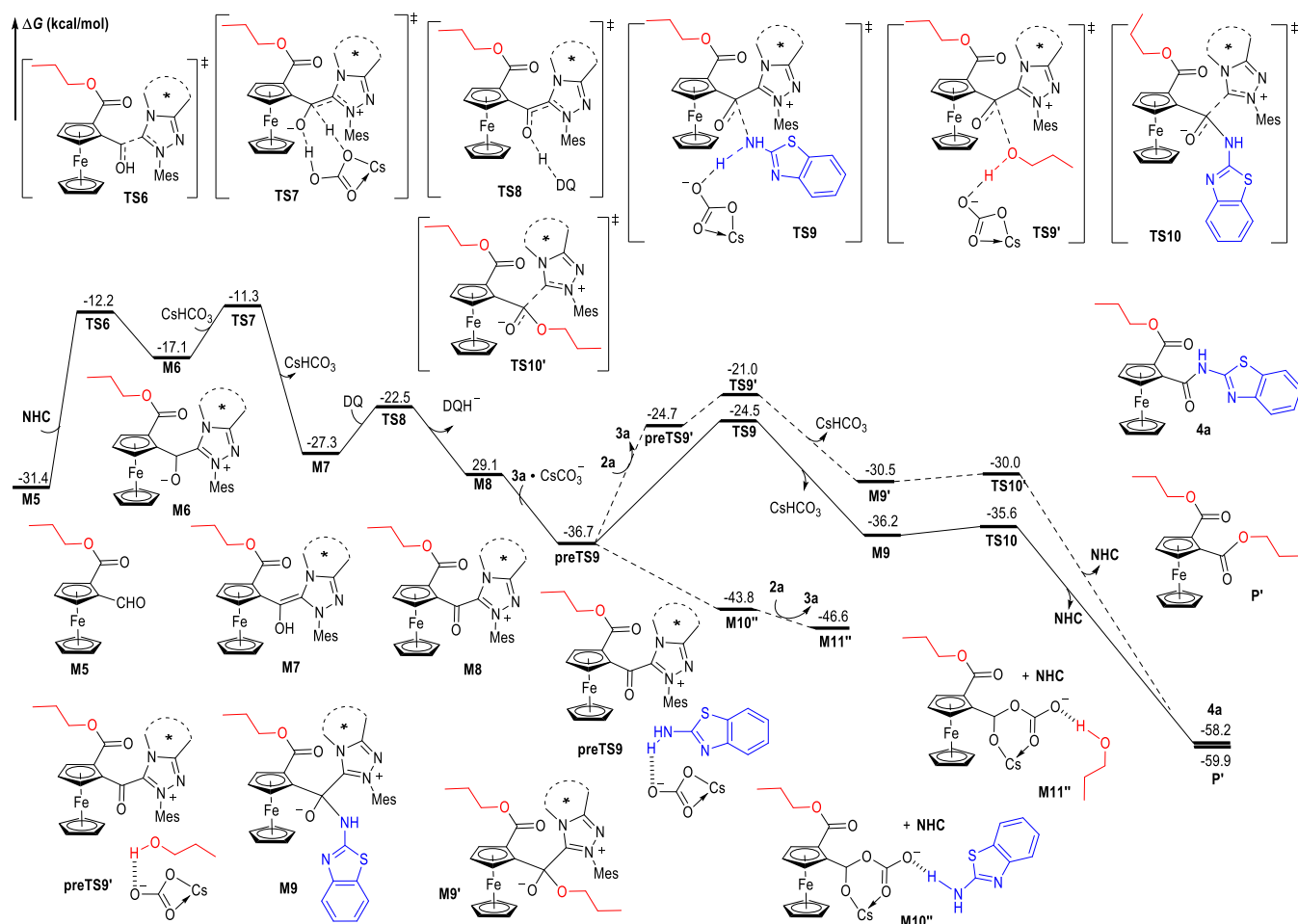


Figure 5. Gibbs free energy profiles for the NHC-catalyzed esterification/amidation relay in the second stage.

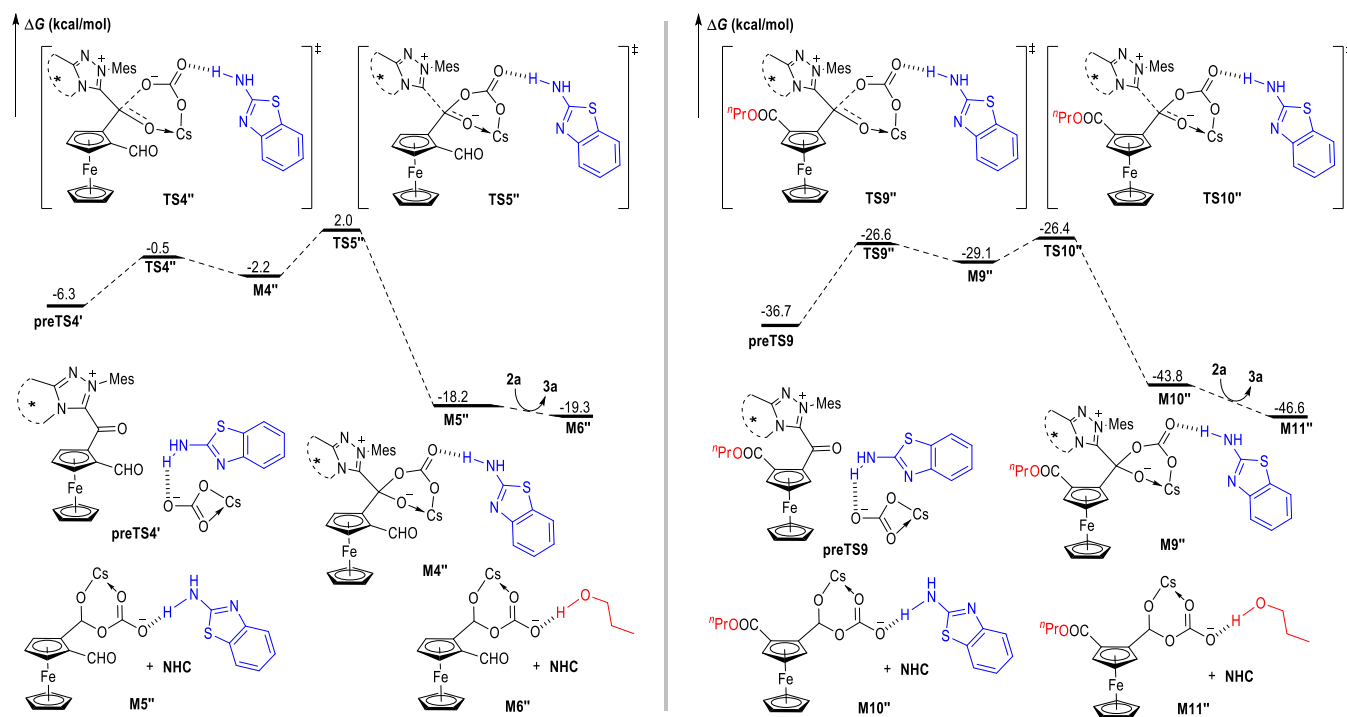


Figure 6. Gibbs free energy profiles for the nucleophilic addition of acylazolium intermediates with CsCO₃.

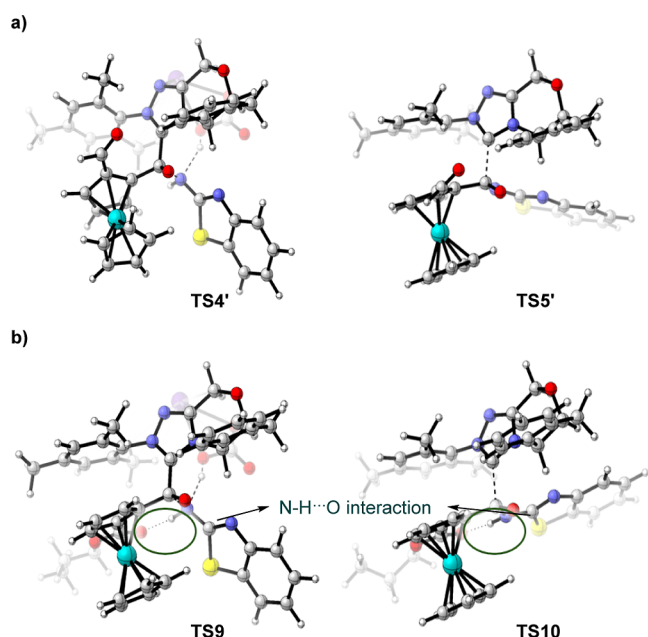


Figure 7. Geometric configurations of oxidative amidation transition states in the two stages. (a) Oxidative amidation process in the first stage. (b) Oxidative amidation process in the second stage.

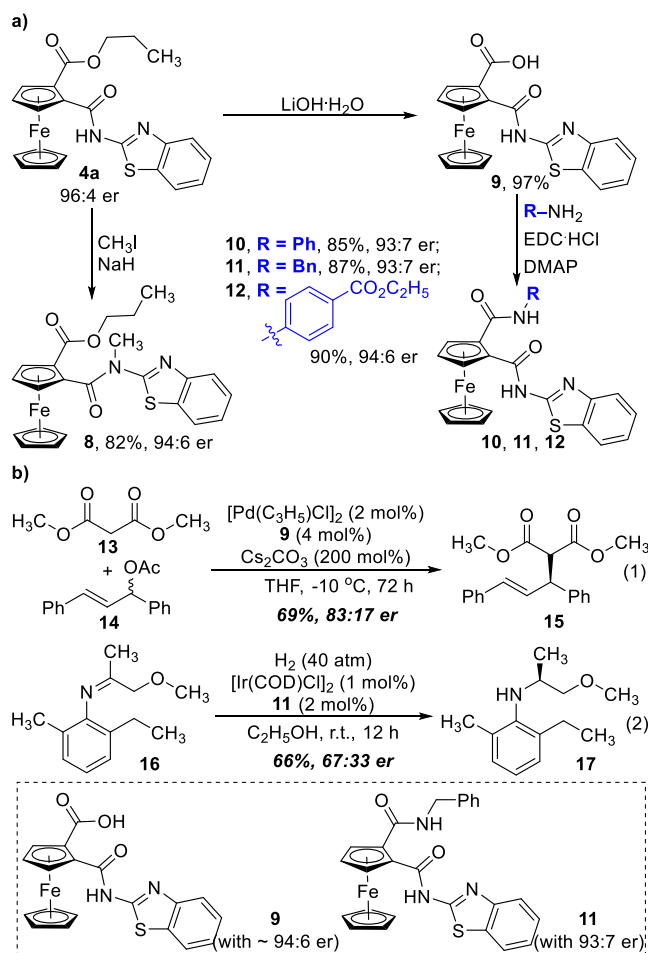


Figure 8. Synthetic applications of the ferrocene-based planar chiral products. (a) Synthetic transformations of the planar chiral product 4a. (b) Practical applications of the planar chiral functional molecules.

Table 2. In Vitro Inhibitive Activities of Planar Chiral Ferrocene Derivatives against *Xoo*^a

compounds	<i>Xoo</i> inhibition rate [%]	
	100 μ g/mL	50 μ g/mL
rac-4p	67.25 \pm 2.57	55.74 \pm 2.13
R _p -4p	86.97 \pm 1.23	57.91 \pm 4.59
S _p -4p	64.54 \pm 3.71	48.33 \pm 2.36
rac-4v	80.84 \pm 3.51	62.25 \pm 3.11
R _p -4v	88.84 \pm 4.09	67.97 \pm 1.78
S _p -4v	60.24 \pm 3.71	47.26 \pm 3.22
rac-5c	62.96 \pm 0.79	49.87 \pm 1.62
R _p -5c	77.64 \pm 4.11	60.83 \pm 2.14
S _p -5c	54.58 \pm 3.74	39.29 \pm 2.69
BT ^b	63.76 \pm 1.59	54.15 \pm 2.84
TC ^c	71.13 \pm 3.12	57.56 \pm 1.26

^aAll data were average data of three replicates. *Xoo* = *Xanthomonas oryzae* pv *oryzae*. *Xac* = *X. axonopodis* pv *citri*. ^bBT = Bismethiazol. ^cTC = Thiodiazole Copper.

for facile access to chiral structures bearing multiple stereogenic planes and axes, exploration of the practical applications of the chiral products in asymmetric catalysis, and the discovery of new agrochemicals based on the unprecedented chiral scaffolds.

METHODS

General Procedure for the Preparation of 4/5. The chiral NHC precatalyst **E** (0.04 mmol, 20 mol %), **DQ** (0.24 mmol, 120 mol %), Cs₂CO₃ (0.24 mmol, 120 mol %), ferrocene dicarbaldehydes **1** (0.2 mmol), alcohol **2** (0.4 mmol), and amine **3** (0.3 mmol) were added to a 10 mL vial equipped with a magnetic stir bar. CH₂Cl₂ (2 mL) was added, and the reaction mixture was stirred at room temperature for 24 h, when the substrate **1** was completely consumed (monitored by TLC). The reaction solvent was removed under reduced pressure, and the residue was subjected to column chromatography (petroleum ether/ethyl acetate = 50:1 to 8:1) to give the chiral desired product **4/5**.

ASSOCIATED CONTENT

Data Availability Statement

All data are available from the authors upon request.

Supporting Information

The Supporting Information is available free of charge at <https://pubs.acs.org/doi/10.1021/acscatal.4c07576>.

¹H and ¹³C NMR spectra for all compounds, ¹⁹F NMR spectra for the compounds containing F atoms, HPLC spectra for the racemic and chiral compounds, and additional experimental details, materials, and methods (PDF)

Full experimental details for the preparation of all new compounds and their spectroscopic and chromatographic data generated in this study (CIF)

AUTHOR INFORMATION

Corresponding Authors

Donghui Wei – College of Chemistry, Pingyuan Laboratory, Zhengzhou University, Zhengzhou 450001, China;

orcid.org/0000-0003-2820-282X; Email: donghuiwei@zzu.edu.cn

Zhichao Jin – State Key Laboratory of Green Pesticide, Guizhou University, Guiyang 550025, China; orcid.org/0000-0003-3003-6437; Email: zcjin@gzu.edu.cn

Authors

Youlin Deng – State Key Laboratory of Green Pesticide, Guizhou University, Guiyang 550025, China

Xinghua Wang – College of Chemistry, Pingyuan Laboratory, Zhengzhou University, Zhengzhou 450001, China; orcid.org/0000-0002-9627-0683

Haitao Liu – State Key Laboratory of Green Pesticide, Guizhou University, Guiyang 550025, China

Hui Cai – State Key Laboratory of Green Pesticide, Guizhou University, Guiyang 550025, China

Chaoyang Song – State Key Laboratory of Green Pesticide, Guizhou University, Guiyang 550025, China

Yonggui Robin Chi – State Key Laboratory of Green Pesticide, Guizhou University, Guiyang 550025, China; School of Chemistry, Chemical Engineering, and Biotechnology, Nanyang Technological University, Singapore 637371, Singapore; orcid.org/0000-0003-0573-257X

Complete contact information is available at: <https://pubs.acs.org/10.1021/acscatal.4c07576>

Author Contributions

^{||}Y.D. and X.W. contributed equally to this work.

Notes

The authors declare no competing financial interest. The X-ray crystallographic coordinates for structures of compounds (R_p)-**4s** reported in this study have been deposited at the Cambridge Crystallographic Data Centre (CCDC), under deposition number CCDC 2351667. These data can be obtained free of charge from The CCDC via www.ccdc.cam.ac.uk/data_request/cif.

ACKNOWLEDGMENTS

We acknowledge financial support from the National Key Research and Development Program of China (2022YFD1700300), the National Natural Science Foundation of China (22371057, 32172459), the Science and Technology Department of Guizhou Province (Qiankehejichu-ZK [2021] Key033), the Central Government Guides Local Science and Technology Development Fund Projects [Qiankehezhongyindi (2024)007, (2023)001], the Program of Major Scientific and Technological, Guizhou Province [Qiankehechengguo(2024) zhongda007], Yongjiang Plan for Innovation and Entrepreneurship Leading Talent Project in the City of Nanning (2021005), the 10 Talent Plan (Shicengci) of Guizhou Province ([2016]5649), the Program of Introducing Talents of Discipline to Universities of China (111 Program, D20023) at Guizhou University, Singapore National Research Foundation under its NRF Investigatorship (NRF-NRFI2016-06), and Competitive Research Program (NRF-CRP22-2019-0002), the Ministry of Education, Singapore, under its MOE AcRF Tier 1 Award (RG7/20, RGS/19), MOE AcRF Tier 2 (MOE2019-T2-2-117), and MOE AcRF Tier 3 Award (MOE2018-T3-1-003).

REFERENCES

(1) Van Staveren, D. R.; Metzler-Nolte, N. Bioorganometallic Chemistry of Ferrocene. *Chem. Rev.* **2004**, *104*, 5931–5985.

(2) Sharma, B.; Kumar, V. Has Ferrocene Really Delivered Its Role in Accentuating the Bioactivity of Organic Scaffolds? *J. Med. Chem.* **2021**, *64*, 16865–16921.

(3) Braga, S. S.; Silva, A. M. S. A New Age for Iron: Antitumoral Ferrocenes. *Organometallics* **2013**, *32*, 5626–5639.

(4) Babin, V. N.; Belousov, Y. A.; Borisov, V. I.; Gumenyuk, V. V.; Nekrasov, Y. S.; Ostrovskaya, L. A.; Sviridova, I. K.; Sergeeva, N. S.; Simenel, A. A.; Snegur, L. V. Ferrocenes as Potential Anticancer Drugs. Facts and Hypotheses. *Russ. Chem. Bull.* **2014**, *63*, 2405–2422.

(5) Sansook, S.; Hassell-Hart, S.; Ocasio, C.; Spencer, J. Ferrocenes in Medicinal Chemistry; a Personal Perspective. *J. Organomet. Chem.* **2020**, *905*, 121017.

(6) Biot, C.; Glorian, G.; Maciejewski, L. A.; Brocard, J. S.; Domarle, O.; Blampain, G.; Millet, P.; Georges, A. J.; Abessolo, H.; Dive, D.; et al. Synthesis and Antimalarial Activity in Vitro and in Vivo of a New Ferrocene-Chloroquine Analogue. *J. Med. Chem.* **1997**, *40*, 3715–3718.

(7) Domarle, O.; Blampain, G.; Agnani, H.; Nzadiyabi, T.; Lebibi, J.; Brocard, J.; Maciejewski, L.; Biot, C.; Georges, A. J.; Millet, P. In Vitro Antimalarial Activity of a New Organometallic Analog, Ferrocenechloroquine. *Antimicrob. Agents Chemother.* **1998**, *42*, 540–544.

(8) Jaouen, G. *Bioorganometallics: Biomolecules, Labelling, Medicine*; Wiley, 2006.

(9) Nesmeyanov, A. N.; Bogomolova, L. G.; Kochetkova, N. S.; Vilchevskaya, V. D.; Palitsyn, N. P.; Andrianova, I. G.; Belozero, O. P. Drug for Anemia and Ozena. USSR Patent 263807, 1966.

(10) Chellan, P.; Sadler, P. J. Enhancing the Activity of Drugs by Conjugation to Organometallic Fragments. *Chem.—Eur. J.* **2020**, *26*, 8676–8688.

(11) McCarthy, J. S.; Rückle, T.; Djeriou, E.; Cantalloube, C.; Ter-Minassian, D.; Baker, M.; O'Rourke, P.; Griffin, P.; Marquart, L.; Hooft van Huijsduijnen, R.; Möhrle, J. J. A Phase II Pilot Trial to Evaluate Safety and Efficacy of Ferroquine Against Early Plasmodium Falciparum in an Induced Blood-Stage Malaria Infection Study. *Malar. J.* **2016**, *15*, 469.

(12) Zhou, Q.-L. *Privileged Chiral Ligands and Catalysts*; Wiley, 2011.

(13) Ye, B.; Cramer, N. Chiral Cyclopentadienyl Ligands as Stereocontrolling Element in Asymmetric C-H Functionalization. *Science* **2012**, *338*, 504–506.

(14) Togni, A.; Hayashi, T. *Ferrocenes*; Wiley, 1995.

(15) Dai, L.-X.; Hou, X.-L. *Chiral Ferrocenes in Asymmetric Catalysis*; Wiley, 2010.

(16) Fu, G. C. Applications of Planar-Chiral Heterocycles as Ligands in Asymmetric Catalysis. *Acc. Chem. Res.* **2006**, *39*, 853–860.

(17) Caniparoli, U.; Escofet, I.; Echavarren, A. M. Planar Chiral 1,3-Disubstituted Ferrocenyl Phosphine Gold(I) Catalysts. *ACS Catal.* **2022**, *12*, 3317–3322.

(18) Halterman, R. L. Synthesis and Applications of Chiral Cyclopentadienylmetal Complexes. *Chem. Rev.* **1992**, *92*, 965–994.

(19) Fu, G. C. Enantioselective Nucleophilic Catalysis with “Planar Chiral” Heterocycles. *Acc. Chem. Res.* **2000**, *33*, 412–420.

(20) Dai, L.-X.; Tu, T.; You, S.-L.; Deng, W.-P.; Hou, X.-L. Asymmetric Catalysis with Chiral Ferrocene Ligands. *Acc. Chem. Res.* **2003**, *36*, 659–667.

(21) Colacot, T. J. A Concise Update on the Applications of Chiral Ferrocenyl Phosphines in Homogeneous Catalysis Leading to Organic Synthesis. *Chem. Rev.* **2003**, *103*, 3101–3118.

(22) Fu, G. C. Asymmetric Catalysis with “Planar-Chiral” Derivatives of 4-(Dimethylamino)pyridine. *Acc. Chem. Res.* **2004**, *37*, 542–547.

(23) Togni, A. Planar-Chiral Ferrocenes: Synthetic Methods and Applications. *Angew. Chem., Int. Ed.* **1996**, *35*, 1475–1477.

(24) Richards, C. J.; Locke, A. J. Recent Advances in the Generation of Non-Racemic Ferrocene Derivatives and Their Application to Asymmetric Synthesis. *Tetrahedron: Asymmetry* **1998**, *9*, 2377–2407.

- (25) Gómez Arrayás, R.; Adrio, J.; Carretero, J. C. Recent Applications of Chiral Ferrocene Ligands in Asymmetric Catalysis. *Angew. Chem., Int. Ed.* **2006**, *45*, 7674–7715.
- (26) Togni, A.; Breutel, C.; Schnyder, A.; Spindler, F.; Landert, H.; Tijani, A. A Novel Easily Accessible Chiral Ferrocenyldiphosphine for Highly Enantioselective Hydrogenation, Allylic Alkylation, and Hydroboration Reactions. *J. Am. Chem. Soc.* **1994**, *116*, 4062–4066.
- (27) Cleveger, A. L.; Stolley, R. M.; Aderibigbe, J.; Louie, J. Trends in the Usage of Bidentate Phosphines as Ligands in Nickel Catalysis. *Chem. Rev.* **2020**, *120*, 6124–6196.
- (28) Check, C. T.; Jang, K. P.; Schwamb, C. B.; Wong, A. S.; Wang, M. H.; Scheidt, K. A. Ferrocene-Based Planar Chiral Imidazopyridinium Salts for Catalysis. *Angew. Chem., Int. Ed.* **2015**, *54*, 4264–4268.
- (29) Qi, H.; Hang, N. N.; Ming, J. Synthesis of Planar Chiral Ferrocenes by Catalytic Desymmetrization Reactions. *ChemCatChem* **2024**, No. e202400736.
- (30) Gao, D.-W.; Shi, Y.-C.; Gu, Q.; Zhao, Z.-L.; You, S.-L. Enantioselective Synthesis of Planar Chiral Ferrocenes via Palladium-Catalyzed Direct Coupling with Arylboronic Acids. *J. Am. Chem. Soc.* **2013**, *135*, 86–89.
- (31) Pi, C.; Cui, X.; Liu, X.; Guo, M.; Zhang, H.; Wu, Y. Synthesis of Ferrocene Derivatives with Planar Chirality via Palladium-Catalyzed Enantioselective C–H Bond Activation. *Org. Lett.* **2014**, *16*, 5164–5167.
- (32) Liu, Y.-H.; Li, P.-X.; Yao, Q.-J.; Zhang, Z.-Z.; Huang, D.-Y.; Le, M. D.; Song, H.; Liu, L.; Shi, B.-F. Cp*Co(III)/MPAA-Catalyzed Enantioselective Amidation of Ferrocenes Directed by Thioamides under Mild Conditions. *Org. Lett.* **2019**, *21*, 1895–1899.
- (33) Wang, Q.; Nie, Y.-H.; Liu, C.-X.; Zhang, W.-W.; Wu, Z.-J.; Gu, Q.; Zheng, C.; You, S.-L. Rhodium(III)-Catalyzed Enantioselective C–H Activation/Annulation of Ferrocenecarboxamides with Internal Alkynes. *ACS Catal.* **2022**, *12*, 3083–3093.
- (34) Zou, X.; Li, Y.; Ke, Z.; Xu, S. Chiral Bidentate Boryl Ligand-Enabled Iridium-Catalyzed Enantioselective Dual C–H Borylation of Ferrocenes: Reaction Development and Mechanistic Insights. *ACS Catal.* **2022**, *12*, 1830–1840.
- (35) Zhou, L.; Cheng, H.-G.; Li, L.; Wu, K.; Hou, J.; Jiao, C.; Deng, S.; Liu, Z.; Yu, J.-Q.; Zhou, Q. Synthesis of Planar Chiral Ferrocenes via Enantioselective Remote C–H Activation. *Nat. Chem.* **2023**, *15*, 815–823.
- (36) Kuang, X.; Li, J.-J.; Liu, T.; Ding, C.-H.; Wu, K.; Wang, P.; Yu, J.-Q. Cu-mediated Enantioselective C–H Alkynylation of Ferrocenes with Chiral BINOL Ligands. *Nat. Commun.* **2023**, *14*, 7698.
- (37) Liu, C.-X.; Xie, P.-P.; Zhao, F.; Wang, Q.; Feng, Z.; Wang, H.; Zheng, C.; You, S.-L. Explicit Mechanism of Rh(I)-Catalyzed Asymmetric C–H Arylation and Facile Synthesis of Planar Chiral Ferrocenophanes. *J. Am. Chem. Soc.* **2023**, *145*, 4765–4773.
- (38) Liu, C. X.; Zhao, F.; Feng, Z.; Wang, Q.; Gu, Q.; You, S. L. Kinetic Resolution of Planar Chiral Metallocenes using Rh-Catalyzed Enantioselective C–H Arylation. *Nat. Synth.* **2023**, *2*, 49–57.
- (39) Huang, F.-R.; Zhang, P.; Yao, Q.-J.; Shi, B.-F. Construction of Planar Chiral Ferrocenes by Cobalt-Catalyzed Enantioselective C–H Acyloxylation Enabled by Dual Ligands. *CCS Chem.* **2024**, *6*, 2783–2793.
- (40) Zheng, Y.; Xie, P.-P.; Zheng, C.; You, S.-L. Cobalt-Catalyzed Asymmetric Synthesis of Planar Chiral Ferrocene Derivatives via C(sp²)–C(sp³) Bond Formation. *CCS Chem.* **2024**, *1*.
- (41) Lv, X.; Wang, M.; Zhao, Y.; Shi, Z. P. (III)-Directed Asymmetric C–H Arylation toward Planar Chiral Ferrocenes by Palladium Catalysis. *J. Am. Chem. Soc.* **2024**, *146*, 3483–3491.
- (42) Zhang, Z.-Z.; Zhou, G.; Yue, Q.; Yao, Q.-J.; Shi, B.-F. Copper/BINOL-Catalyzed Enantioselective C–H Functionalization toward Planar Chiral Ferrocenes Under Mild Conditions. *ACS Catal.* **2024**, *14*, 4030–4039.
- (43) Liu, L.; Liu, H.; Zuo, Z.; Zhang, A.-A.; Li, Z.; Meng, T.; Wu, W.; Hua, Y.; Mao, G. Synthesis of Planar Chiral Isoquinolinone-Fused Ferrocenes through Palladium-Catalyzed C–H Functionalization Reaction. *Chin. Chem. Lett.* **2021**, *32*, 239–242.
- (44) Schaarschmidt, D.; Lang, H. Selective Syntheses of Planar-Chiral Ferrocenes. *Organometallics* **2013**, *32*, 5668–5704.
- (45) Yang, Y.; Hang, N.-N.; Liu, H.-Y.; Chen, S.; Ming, J. Single-Step Construction of Planar and Central Chirality in Metallocenes by Rhodium-Catalyzed Desymmetric Cyclization. *ACS Catal.* **2023**, *13*, 12464–12471.
- (46) Lv, X.; Xu, J.; Sun, C.; Su, F.; Cai, Y.; Jin, Z.; Chi, Y. R. Access to Planar Chiral Ferrocenes via N-Heterocyclic Carbene-Catalyzed Enantioselective Desymmetrization Reactions. *ACS Catal.* **2022**, *12*, 2706–2713.
- (47) Liu, Q.; Teng, K.; Zhang, Y.; Lv, Y.; Chi, Y. R.; Jin, Z. Chemodivergent Parallel Kinetic Resolution of Paracyclophanes: Enantiomer Fishing with Different Substrates. *Angew. Chem., Int. Ed.* **2024**, *63*, No. e202406386.
- (48) Lv, X.; Su, F.; Long, H.; Lu, F.; Zeng, Y.; Liao, M.; Che, F.; Wu, X.; Chi, Y. R. Carbene Organic Catalytic Planar Enantioselective Macrolactonization. *Nat. Commun.* **2024**, *15*, 958.
- (49) Samanta, R. C.; De Sarkar, S.; Fröhlich, R.; Grimme, S.; Studer, A. N-Heterocyclic Carbene (NHC) Catalyzed Chemoselective Acylation of Alcohols in the Presence of Amines with Various Acylating Reagents. *Chem. Sci.* **2013**, *4*, 2177–2184.
- (50) Zhang, Y.; Cai, H.; Gan, X.; Jin, Z. N.-N-Heterocyclic carbene-catalyzed enantioselective (dynamic) kinetic resolutions and desymmetrizations. *Sci. China:Chem.* **2024**, *67*, 482–511.
- (51) Zhang, M.; Yang, X.; Peng, X.; Li, X.; Jin, Z. Asymmetric Construction of Axial and Planar Chirality with N-Heterocyclic Carbene (NHC) Organocatalysis. *Sci. China:Chem.* **2024**, *68*, 815–825.
- (52) Huang, Z.; Huang, X.; Li, B.; Mou, C.; Yang, S.; Song, B. A.; Chi, Y. R. Access to P-Stereogenic Phosphinates via N-Heterocyclic Carbene-Catalyzed Desymmetrization of Bisphenols. *J. Am. Chem. Soc.* **2016**, *138*, 7524–7527.
- (53) Li, B. S.; Wang, Y.; Proctor, R. S.; Jin, Z.; Chi, Y. R. Carbene-catalyzed Desymmetrization of 1,3-Diols: Access to Optically Enriched Tertiary Alkyl Chlorides. *Chem. Commun.* **2016**, *52*, 8313–8316.
- (54) Wu, Z.; Wang, J. Enantioselective Medium-Ring Lactone Synthesis through an NHC-Catalyzed Intramolecular Desymmetrization of Prochiral 1,3-Diols. *ACS Catal.* **2017**, *7*, 7647–7652.
- (55) Lu, S.; Song, X.; Poh, S. B.; Yang, H.; Wong, M. W.; Zhao, Y. Access to Enantiopure Triarylmethanes and 1,1-Diaryllkanes by NHC-Catalyzed Acylative Desymmetrization. *Chem.—Eur. J.* **2017**, *23*, 2275–2281.
- (56) Li, S.; Liu, B.; Chen, L.; Li, X.; Cheng, J.-P. N.-N-Heterocyclic carbene promoted enantioselective desymmetrization reaction of diarylalkane-bisphenols. *Org. Chem. Front.* **2018**, *5*, 1101–1107.
- (57) Zhuo, S.; Zhu, T.; Zhou, L.; Mou, C.; Chai, H.; Lu, Y.; Pan, L.; Jin, Z.; Chi, Y. R. Access to All-Carbon Spirocycles through a Carbene and Thiourea Cocatalytic Desymmetrization Cascade Reaction. *Angew. Chem., Int. Ed.* **2019**, *58*, 1784–1788.
- (58) Zhu, T.; Liu, Y.; Smetankova, M.; Zhuo, S.; Mou, C.; Chai, H.; Jin, Z.; Chi, Y. R. Carbene-Catalyzed Desymmetrization and Direct Construction of Arenes with All-Carbon Quaternary Chiral Center. *Angew. Chem., Int. Ed.* **2019**, *58*, 15778–15782.
- (59) Yang, G.; Guo, D.; Meng, D.; Wang, J. NHC-Catalyzed Atropenantioselective Synthesis of Axially Chiral Biaryl Amino Alcohols via a Cooperative Strategy. *Nat. Commun.* **2019**, *10*, 3062.
- (60) Lu, S.; Poh, S. B.; Rong, Z. Q.; Zhao, Y. NHC-Catalyzed Atroposelective Acylation of Phenols: Access to Enantiopure NOBIN Analogs by Desymmetrization. *Org. Lett.* **2019**, *21*, 6169–6172.
- (61) Di Carmine, G.; Ragno, D.; Brandolese, A.; Bortolini, O.; Pecorari, D.; Sabuzi, F.; Mazzanti, A.; Massi, A. Enantioselective Desymmetrization of 1,4-Dihydropyridines by Oxidative NHC Catalysis. *Chem.—Eur. J.* **2019**, *25*, 7469–7474.
- (62) Barik, S.; Shee, S.; Das, S.; Gonnade, R. G.; Jindal, G.; Mukherjee, S.; Biju, A. T. NHC-Catalyzed Desymmetrization of N-Aryl Maleimides Leading to the Atroposelective Synthesis of N-Aryl Succinimides. *Angew. Chem., Int. Ed.* **2021**, *60*, 12264–12268.

- (63) Zhao, W.; Liu, J.; He, X.; Jiang, H.; Lu, L.; Xiao, W. N-Heterocyclic Carbene (NHC)-Catalyzed Desymmetrization of Biaryldialdehydes to Construct Axially Chiral Aldehydes. *Chin. J. Org. Chem.* **2022**, *42*, 2504.
- (64) Zhou, M.; Liu, J.; Deng, R.; Wang, Q.; Wu, S.; Zheng, P.; Chi, Y. R. Construction of Tetrasubstituted Silicon-Stereogenic Silanes via Conformational Isomerization and N-Heterocyclic Carbene-Catalyzed Desymmetrization. *ACS Catal.* **2022**, *12*, 7781–7788.
- (65) Liu, J.; Zhou, M.; Deng, R.; Zheng, P.; Chi, Y. R. Chalcogen Bond-Guided Conformational Isomerization Enables Catalytic Dynamic Kinetic Resolution of Sulfoxides. *Nat. Commun.* **2022**, *13*, 4793.
- (66) Liu, H.; He, P.; Liao, X.; Zhou, Y.; Chen, X.; Ou, W.; Wu, Z.; Luo, C.; Yang, L.; Xu, J. Stereoselective Access to Silicon-Stereogenic Silacycles via the Carbene-Catalyzed Desymmetric Benzoin Reaction of Siladials. *ACS Catal.* **2022**, *12*, 9864–9871.
- (67) Pi, C.; Li, Y.; Cui, X.; Zhang, H.; Han, Y.; Wu, Y. Redox of Ferrocene Controlled Asymmetric Dehydrogenative Heck Reaction via Palladium-Catalyzed dual C–H Bond Activation. *Chem. Sci.* **2013**, *4*, 2675–2679.
- (68) Zhang, Q.; Cui, X.; Zhang, L.; Luo, S.; Wang, H.; Wu, Y. Redox Tuning of a Direct Asymmetric Aldol Reaction. *Angew. Chem., Int. Ed.* **2015**, *54*, 5210–5213.
- (69) Zhang, H.; Cui, X.; Yao, X.; Wang, H.; Zhang, J.; Wu, Y. Directly Fused Highly Substituted Naphthalenes via Pd-Catalyzed Dehydrogenative Annulation of N, N-Dimethylaminomethyl Ferrocene using a Redox Process with a Substrate. *Org. Lett.* **2012**, *14*, 3012–3015.
- (70) Huang, Y.; Pi, C.; Cui, X.; Wu, Y. Palladium(II)-Catalyzed Enantioselective C–H Alkenylation of Ferrocenecarboxylic Acid. *Adv. Synth. Catal.* **2020**, *362*, 1385–1390.
- (71) For the pKa values of various amines, see: <https://www.chemicalbook.com/ProductIndex.aspx> (accessed Jan 15, 2025).
- (72) Zhuo, L. G.; Liao, W.; Yu, Z. X. A Frontier Molecular Orbital Theory Approach to Understanding the Mayr Equation and to Quantifying Nucleophilicity and Electrophilicity by Using HOMO and LUMO Energies. *Asian J. Org. Chem.* **2012**, *1*, 336–345.
- (73) Mayr, H.; Kempf, B.; Ofial, A. R. π -Nucleophilicity in Carbon–carbon Bond-Forming Reactions. *Acc. Chem. Res.* **2003**, *36*, 66–77.
- (74) Du, L.; Cao, P.; Xing, J.; Lou, Y.; Jiang, L.; Li, L.; Liao, J. Hydrogen-Bond-Promoted Palladium Catalysis: Allylic Alkylation of Indoles with Unsymmetrical 1,3-Disubstituted Allyl Acetates Using Chiral Bis(sulfoxide) Phosphine Ligands. *Angew. Chem., Int. Ed.* **2013**, *52*, 4207–4211.
- (75) Cheng, J.; Huang, Z.; Chi, Y. R. NHC Organocatalytic Formal LUMO Activation of α , β -Unsaturated Esters for Reaction with Enamides. *Angew. Chem.* **2013**, *125*, 8754–8758.
- (76) Blaser, H.-U.; Brieden, W.; Pugin, B.; Spindler, F.; Studer, M.; Togni, A. Solvias Josiphos Ligands: From Discovery to Technical Applications. *Top. Catal.* **2002**, *19*, 3–16.
- (77) Blaser, H. U.; Pugin, B.; Spindler, F. Progress in Enantioselective Catalysis Assessed from an Industrial Point of View. *J. Mol. Catal. A: Chem.* **2005**, *231*, 1–20.
- (78) Kuremoto, T.; Yasukawa, T.; Kobayashi, S. Continuous-Flow Asymmetric Hydrogenation for the Synthesis of an (S)-Metolachlor Intermediate Using Catalysts Immobilized on a Core/Shell-Type Support. *Adv. Synth. Catal.* **2024**, *366*, 757–761.
- (79) Bai, S.; Zhang, M.; Tang, S.; Li, M.; Wu, R.; Wan, S.; Chen, L.; Wei, X.; Li, F. Research Progress on Benzimidazole Fungicides: A Review. *Molecules* **2024**, *29*, 1218.
- (80) Xu, C.; Liang, X.; Hou, Y.; Zhou, M. Effects of the Novel Fungicide Benzothiostrubin on *Sclerotinia sclerotiorum* in the Laboratory and on *Sclerotinia* Stem Rot in Rape Fields. *Plant Dis.* **2015**, *99*, 969–975.
- (81) Adhikari, T. B.; Cruz, C.; Zhang, Q.; Nelson, R. J.; Skinner, D. Z.; Mew, T. W.; Leach, J. E. Genetic Diversity of *Xanthomonas oryzae* pv. *oryzae* in Asia. *Appl. Environ. Microbiol.* **1995**, *61*, 966–971.
- (82) Niño-Liu, D. O.; Ronald, P. C.; Bogdanove, A. J. *Xanthomonas oryzae* Pathovars: Model Pathogens of a Model Crop. *Mol. Plant Pathol.* **2006**, *7*, 303–324.
- (83) Sakthivel, K.; Kumar, A.; Gautam, R. K.; Manigundan, K.; Laha, G. S.; Velazhahan, R.; Singh, R.; Yadav, I. S. Intra-Regional Diversity of Rice Bacterial Blight Pathogen, *Xanthomonas oryzae* pv. *oryzae*, in the Andaman Islands, India: Revelation by Pathotyping and Multilocus Sequence Typing. *J. Appl. Microbiol.* **2021**, *130*, 1259–1272.